RSC Advances

ROYAL SOCIETY OF CHEMISTRY

www.rsc.org/advances

Journal Name

ARTICLE

High performance of P (VDF-HFP)/Ag@TiO_2 hybrid films with enhanced dielectric permittivity and low dielectric loss

Received 00th January 20xx,
Accepted 00th January 20xx

DOI: 10.1039/x0xx00000x

www.rsc.org/

Xingrong Xiao, Hui Yang , Nuoxin Xu, Liang Hu and Qilong Zhang*

Ag@TiO_2 core-shell nanoparticles were synthesized as fillers using a simple vapor-thermal method. Based on the nanoparticles, the P (VDF-HFP)/Ag@TiO_2 hybrid films were first prepared by embedding Ag@TiO_2 nanoparticles in poly (vinylidene fluoride co-hexafluoropropylene) [P (VDF-HFP)] matrix. Microstructure and thermal analysis confirmed that Ag nanoparticle have been successfully coated by TiO_2 shells and the thickness of shell layer is about 8-10nm. The Ag@TiO_2 nanoparticles act as nucleation sites to promote the crystallization process of polymer matrix without changing its structure. The P (VDF-HFP)/Ag@TiO_2 composite exhibited enhanced dielectric properties over a wide frequency range and the dielectric permittivity of polymer nanocomposites is enhanced by ~300% over the P(VDF-HFP) matrix at a low filler loading of 10vol%. Moreover, the P(VDF-HFP)/Ag@TiO_2 also exhibited higher dielectric constant than P(VDF-HFP)/Ag, P(VDF-HFP)/TiO_2 and P(VDF-HFP)/Ag/TiO_2 blend composite while maintaining a low loss tangent(below 0.03 at 1KHz) for duplex polarizations effect.

Introduction

Polymer materials with high dielectric constant achieved continuous attention in electronic and electrical industry due to their inherent advantages in flexibility, easy processing, and high breakdown strength [1-3]. However, most general polymers show a low dielectric constant. Poly (vinylidene fluoride) (PVDF), and copolymers such as trifluoroethylene (P(VDF-TrFE)) and hexafluoropropylene (P (VDF-HFP)) , are usually employed as the polymer matrix because of their high dielectric constants[8-10]. Methods for enhancing the dielectric constant of polymers have received increasing attention in recent years [1].

Basically, two methods have been utilized to prepare polymer composites with high dielectric constant. One method to increase the dielectric constant is to introducing ceramics particles (such as $BaTiO_3$, (Ba, Sr)TiO_3, Pb(Zr, Ti)O_3, $CaCu_3Ti_4O_{12}$) with high dielectric constants into the polymer matrix[4-12]. However, the permittivity can only be enhanced under certain content of ceramics fillers, usually at a typical volume loading of 30vol%-50vol%, which result in poor mechanical flexibility, large loss and poor insulation properties [13]. Another strategy focuses on incorporating conductive fillers such as silver, copper, reduced graphene oxide, and carbon-nanotube into the polymer matrix near the percolation threshold to achieve an increase of dielectric constant [14-17]. Among the conductive fillers, silver nanoparticles and nanofibers have aroused much interest because of their excellent thermal, electric and optical properties. Many Ag/polymer studies have been performed. However, a remarkable improvement in the permittivity by introducing conductive filler including Ag is also accompanied by larger dielectric loss which limits the application of the composite materials.

Currently, it's still a challenge work to raise dielectric permittivity of polymer by preparing conductive filler-polymer composites while retaining a low loss tangent [18]. To solve this problem, surfactant treatments or modification by a coupling agent and multi-level nanostructure engineering has become research focus [19-23]. Zhang et al. reported a dielectric composite with core-shell structured Ag nanoparticles@polydopamine as fillers and PVDF as polymer matrix, and the hybrid film achieved the highest dielectric constant (~53) and relative low dielectric loss (~0.53) with 25wt. % filler loading at 100Hz [20]. Zheng et al. prepared the nanocomposite with Ag nanowires embedded in PVDF; the composite film exhibits a high dielectric constant (379) and low loss (0.15) at 1000 Hz as the relatively high filler concentration (20vol. %) of Ag nanowires [21]. Kuang et al reported the Ag@C/PVDF composite with a dielectric permittivity of around 11.7, while the loss is 0.08 at 1 KHz [22]. Liang and co-workers introduced Ag@SiO_2 nanoparticles into $BaTiO_3$/PVDF matrix and achieved high permittivity with relatively low loss of 0.82[23].

In this paper, we design the Ag@TiO_2 core-shell nanostructure film to improve dielectric properties of P (VDF-HFP) polymer. Surface-functionalized Ag nanoparticles with a TiO_2 coating were synthesized by a simple vapor-thermal method and used as fillers to prepare P (VDF-HFP)-based composites. The results indicated that the prepared P (VDF-HFP)/ Ag@TiO_2 composites exhibit higher dielectric constant than pure Ag/P (VDF-HFP) composite while maintaining a low loss tangent (below 0.03 at 1000Hz).

Experimental

Materials

Principal materials include Ag nanopowders (<100nm particle size, contains PVP as dispersant, 99.5% trace metals basis, Sigma-Aldrich), Poly(vinylidene fluoride-co-hexafluoropylene) (P(VDF-HFP), pellets, Sigma-Aldrich), tetrabutyl titanate (TBOT, >99.0%, Aladdin, China), titanium dioxide(TiO_2, 100nm, anatase, Aladdin, China) N, N-dimethyl formamide (DMF, Aladdin, China), Ethanol(Sinopharm Chemical Reagent Co.,Ltd). All of the chemicals were used as-received without any further treatment.

Preparation of the Ag@TiO_2 core–shell nanoparticles

The Ag@TiO_2 core–shell powder was prepared by the vapor-thermal method using TBOT as titanium source [24-26]. In a typical procedure, 0.5g Ag powder was dispersed in the mixed solution made by ethanol (25mL) and TBOT (180μL), and the mixed solution was pour into a 50mL Teflon container, which was then placed into a 200mL stainless steel autoclave with a Teflon liner. The gap between the two liner walls was filled with distilled water to avoid contact with TBOT directly. The autoclave was sealed and heated to 150 °C for 10 h. During the reaction, distilled water vaporized and contacted with TBOT, which resulted in its hydrolysis. The autoclave was cooled to room temperature after reaction, and the supernatant was removed while the precipitate was repeatedly washed with ethanol for three times, and then dried at 80 °C in a vacuum oven for 8 h.

Preparation of the Ag@TiO_2/P(VDF-HFP) films

For the preparation of Ag@TiO_2/P(VDF-HFP) composite films, P(VDF-HFP) was first dissolved in DMF and stirred for 3h (mass to volume ratio P(VDF-HFP)/DMF=1:10). Then the obtained core-shell nanoparticles were grinded and dispersed into the mixture of DMF and P(VDF-HFP) slowly by ultra-sonication at room temperature for 1 h and stirred for 12 hours to form a stable suspension. The thin films were made by casting the as-synthesized mixture onto the glass substrate and heated in a vacuum oven at 80 °C for 12 h to remove the residual solvent.

Characterization

The phase composition of nanopowders was characterized by powder X-ray diffraction (Lab X, SHIMADZU, XRD-6000) analysis, using Cu *Kα* radiation in the 2θ range of 10° - 90°. Transmission electron microscopy (TEM) images and Energy-dispersive spectroscopy line-scan of coated nanoparticles were obtained from a Tecnai G2 F20 S-TWIN instrument operated at an accelerating voltage of 200 kV, X-ray photoelectron spectroscopy (XPS) was recorded using an ESCALAB 250XI X-ray photoelectron spectrometer (Thermo Fisher Scientific, USA).The cross section morphology of the composites was characterized on a SU-70 field emission scanning electron microscope (SEM) instrument with all samples fractured in the liquid nitrogen before testing. Differential scanning calorimetry (DSC) was performed using a PE-DSC 7 analyser between 30 °C and 200 °C with a heating rate of 10 °C·min^{-1} under a nitrogen atmosphere.

The dielectric properties of the composites were performed on a broadband dielectric spectrometer (NOVOCONTROL GmbH, Germany) with Ag electrodes fabricating on both surfaces of the films. All the measurements were carried out in the frequency range of 10^{-1} to 10^{7} Hz at several temperatures between 20 °C and 100 °C.

Results and Discussions

Figure 1(a) shows the XRD patterns of Ag@TiO_2 core@shell nanoparticles. The 2θ values at 38.180, 44.380, 64.480, 77.80, and 81.50, which correspond to the (111), (200), (220), (311) and (222) crystal planes of face-centered cubic (fcc) silver (JCPDS card no. 4-783, a = 4.08 Å) respectively. There was no obvious characteristic peak of TiO_2 phase observed in the pattern and this implied that the TiO_2 is amorphous or shows low crystallinity compared with Ag nanoparticle. To further confirm the coating results of the composition, TEM analysis was performed on the nanoparticle. Figure 1(b) shows the coating microstructure of the sample. The thickness of the compound coating layer is about 8-10nm while coating coverage is at a high level with fine layer feature. The HRTEM observation is shown in Fig. 1(c), from which can be found that the coating layer showed crystallized phases. The lattice fringes allow for the identification of crystallographic spacing. The fringe spacing of 0.35 and 0.236 nm matches that of the TiO_2 anatase (101) plane and Ag (111) plane, respectively [27, 28]. Energy-dispersive spectroscopy line-scan microanalysis is illustrated in Figure 1(d), which describe the composition distribution of the particle. It can be seen that element Ti is enriched at the edge of the particle. In contrast, Ag was in high content in the core of the particle, where there is also a little element Ti performing co-existence. It indicated that TiO_2 successfully encapsulated the Ag nanoparticles as coating layer in the vapor-thermal process, because TBOT contacted with the water vapor rather than liquid state. This method had limited the hydrolysis rate of TBOT thus avoiding TiO_2 nucleated separately-incorporate and grew.

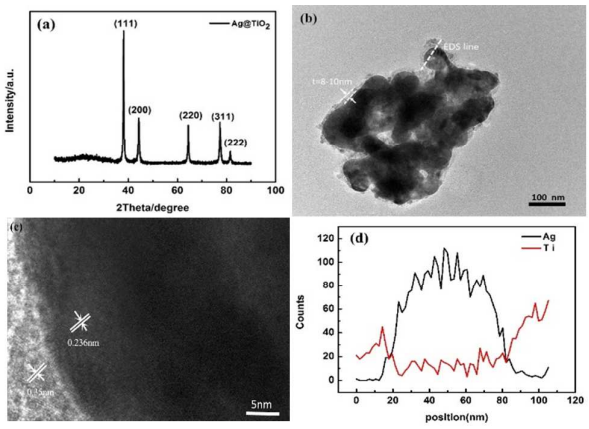

Figure 1(a) XRD pattern of Morphologies of the as-prepared Ag@TiO_2 core@shell. (b) TEM image of coated Ag particle. (c) HRTEM image of the coating layer. (d) EDS results of line-scan micro analysis for the coated Ag particle in figure 1(b).

XPS spectra are tested to analyse the elemental compositions and chemical status of the as-prepared samples. Figure 2(a) shows the XPS survey spectra of Ag@TiO_2. The sample contains mainly Ag,

Ti, and O elements, and a weak carbon emission peak can be observed, which may be caused by the ex situ preparation process and the transfer process of the sample into the UHV chamber [29]. Figure 2(b)-2(d) displays the high-resolution XPS spectrum of element Ag, Ti, O respectively in the Ag@TiO_2 sample. The peaks observed at 368.2 eV and 374.2eV [30] (Figure2b) can be ascribed to Ag $3d_{3/2}$ and Ag $3d_{5/2}$ of the metallic silver. The 6.0 eV difference between the BE of Ag $3d_{5/2}$ and $3d_{3/2}$ peaks is also characteristic of metallic nature Ag 3d states. As no peak was found corresponding to sliver oxide species in XPS and XRD, indicating that Ag cores mainly exist as Ag^0 in the core@shell structure nanoparticles and the chemical state of Ag had not been changed during the reaction. The product exhibit two Ti $2p_{1/2}$ (464.9 eV) and Ti $2p_{3/2}$ (459.2 eV)[31] peaks as shown in Figure 2c, which are assigned to the Ti^{4+} oxidation state according to reported XPS data[32]. As the splitting of the 2p doublet was 5.7 eV, this binding energy also indicated that the TiO_2 existed. The XPS spectra of O1s of the core-shell nanoparticle with an asymmetric characterization (Figure 2d) that can be fitted with the nonlinear least squares fitting program using Gaussian peak shapes. After deconvolution, The O 1s region was fitted into three peaks. The main peak belongs to Ti–O of TiO_2 (530.4 eV)[31], and the minor peak is attributed to the surface hydroxyl group（532.2eV）or defective oxides[33].Usually, hydroxyl groups measured by XPS are ascribed to the chemisorbed H_2O [27]. Some H_2O was easily adsorbed on the surface of TiO_2 powders during the vapor-hydrothermal process; however, this adsorption will be reinforced under the ultrahigh vacuum condition of the XPS system. Therefore, the XPS spectra didn't illustrate completely the peak of physically adsorbed H_2O on the samples. The minimum peak observed is attributed to carbonyl oxygen (533.8eV) of the oxygen chemisorbed [34]. On the basis of the data of Figure 2(a)-(d), it can be concluded that the Ag@TiO_2 core-shell nanoparticles are composted of TiO_2 phase and silver.

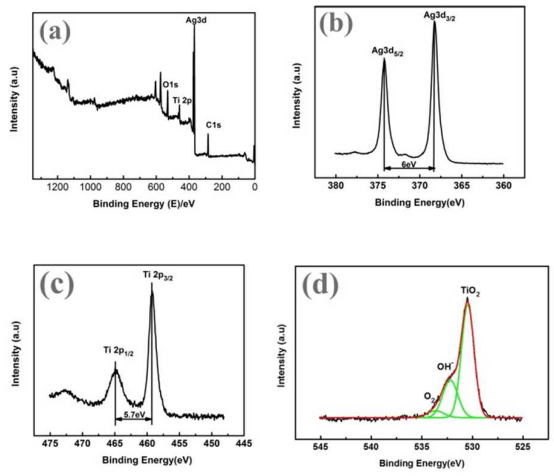

Fig.2 XPS spectra of the nanoparticle (a) survey spectra (b) Ag 3d region (c) Ti 2p region (d) O 1s region

Figure 3 shows SEM images of freeze-fractured cross sections of the films. Figure 3(a) shows the microstructure of the Ag@TiO_2 / P (VDF-HFP) hybrid film with 6vol% concentration, and it shows that P (VDF-HFP) matrix forms a continuous phase. The Ag@TiO_2 nanoparticles are embedded in the P (VDF-HFP) matrix and dispersed relative homogenously because of the low doping concentration. For comparison, Figure 3(b) illustrates the microstructure of the Ag@TiO_2 / P (VDF-HFP) hybrid film with 12vol% concentration. It can be observed that local accumulation occurred and filled large particle clusters formed, therefore, the continuity of P (VDF-HFP) matrix is slightly decreased.

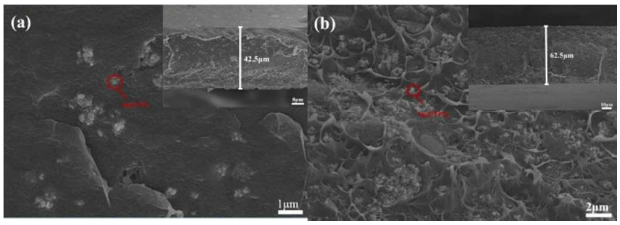

Fig. 3 SEM images of the cross-sectional of films. (a) The film filled with 6vol% Ag@TiO_2. (b) The film filled with 12vol% Ag@TiO_2. Filled inset: typical film thickness

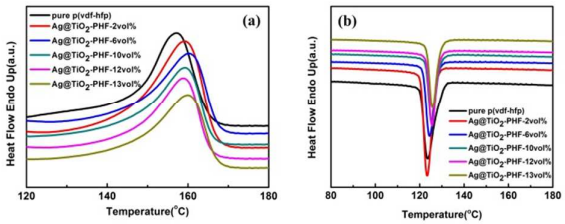

Fig.4 (a) DSC melting curves and (b) cooling curves of pure P(VDF-HFP) and P(VDF-HFP)/ Ag@TiO_2 nanocomposites with different loading level of Ag@TiO_2 nanoparticles.

DSC test was adopted to investigate the effect of Ag@TiO_2 nanoparticles on the crystallization behavior of P (VDF-HFP) matrix after erasing the thermal history. In Figure. 4(a), it can be observed that the melt temperature (Tm) of nanocomposite is obvious higher than pure P (VDF-HFP), which illustrates the nanoparticles impede the melt process of P (VDF-HFP) matrix. The hindering effect is enhanced as the content of particle is increasing at a low fraction (< 10vol %). However, when the content reaches to a higher level (>10vol %), the Tm of the composites was not proportional to content changes, which means the obstacle has no specific relationship with the filling fraction anymore. It is deduced that the effective interfacial area of nanoparticles affects the melt behavior of P (VDF-HFP) to a certain extent [35]. As is shown in Figure. 4(b), the crystallization temperatures (T_c) of the composites obviously shift to high temperatures after the introduction of Ag@TiO_2 nanoparticles. For example, neat P (VDF-HFP) has a low Tc around 123.4 °C; however, Tc is slightly increased by more than 2°C for the composite with 10 vol% Ag@TiO_2 nanoparticles. It has been proven in previous work that the well-dispersed nanofillers in the polymer matrix can act as nucleation sites to promote the crystallization process of polymer matrix without changing its structure [36]. On the other hand, the nanofillers also inhibit the movement of the polymer chain segment, which improved the T_c of polymer composites [37].Therefore, the increment of Tc values for P (VDF-HFP)/ Ag@TiO_2 composites is due to the presence of Ag@TiO_2 nanoparticles. Furthermore, high Tc can be obtained at the

composites with homogenous structure and strong interfacial adhesion between Ag@TiO_2 and the polymer matrix.

Figure. 5(a) presents the dependence of dielectric permittivity of P (VDF-HFP)/Ag@TiO_2 hybrid films on frequency at room temperature. We found that all composites result in significant increment in dielectric constant at a small loading of nanocomposites, the dielectric constant of hybrid film increase continuously with the increasing of Ag@TiO_2 nanoparticles. The dielectric permittivity reaches up to 36 at 13vol% of Ag@TiO_2 nanoparticles, which is nearly four times as pure P (VDF-HFP). As shown in Figure 3, these well-dispersed Ag@TiO_2 nanoparticles are isolated by very thin P (VDF-HFP) layer, forming a number of microcapacitors, which contributes to the high dielectric constant of composites. Moreover, charges can be accumulated at the interfaces between Ag, TiO_2 and polymer matrix due to their different dielectric constant as well as conductivity. It is known that the dielectric properties of composites are closely related to Maxwell-Wagner-Sillars (MWS) interfacial polarization that can make a remarkable contribution to the increment in dielectric permittivity in low frequency range [38, 39]. Here, due to the introduction of TiO_2 interlayer, it is almost unlikely for Ag to form a conductive network through the whole system, and the controlled separation between Ag particles suppressed occurrence of "percolation" in the composites. Thus, with the increasing loading of Ag@TiO_2, more microcapacitors are formed and greater interfacial areas are introduced in the composite, leading to a steady increase of dielectric constant. Meanwhile, the decrease in the dielectric constant with increase in frequency is caused by the slow dielectric relaxation of the matrix and the interface of the composite [40].

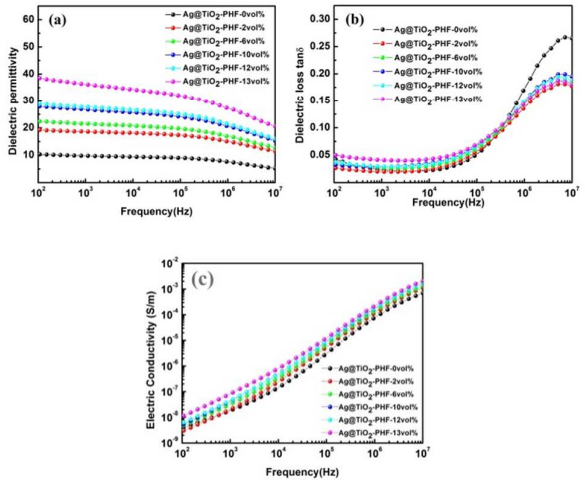

Fig.5 Frequency dependence of (a) dielectric permittivity (b) dielectric loss (tan δ) (c) electrical conductivity of P(VDF-HFP)/Ag@TiO_2 hybrid films at various volume fractions at room temperature.

Figure. 5(b) shows the frequency dependence of loss tangent (tan δ) of P (VDF-HFP)/Ag@TiO_2 hybrid films. As dielectric loss is mainly determined by electrical conduction and dipolar polarization at frequencies larger than 10^4Hz, the low dielectric loss in composites can be attributed to the highly restricted polymer chain motion in the high-frequency range, the dielectric loss peak is attributed to two molecular motions, namely the micro-Brownian moments of the amorphous chain segments and molecular motion on the interfaces (such as amorphous/crystalline interfaces and a/b interfaces)[41]. It is interesting to note that the dielectric loss of P (VDF-HFP)/Ag@TiO_2 composites in the high-frequency range is lower than pure P(VDF-HFP), which may further confirm the pinning effect of nanoparticles to polymer chain and thus develop frequency stability of composites. It further implies the homogenous distribution of the nanoparticles in the P (VDF-HFP) matrix.

Figure. 5(c) shows alternating current (AC) conductivity of P (VDF-HFP)/Ag@TiO_2 composites with different filler contents in the 1×10^2 to 1×10^7 Hz range. It also shows strong frequency dependence of electrical conductivity for the composites in which the conductivity of all samples accelerates linearly with the frequency increasing. In addition, the electrical conductivity of all the composites with Ag@TiO_2 nanoparticles are only slightly higher than that of the pure P (VDF-HFP), indicating that no conductive network was formed and these prepared film showed the good insulation performance.

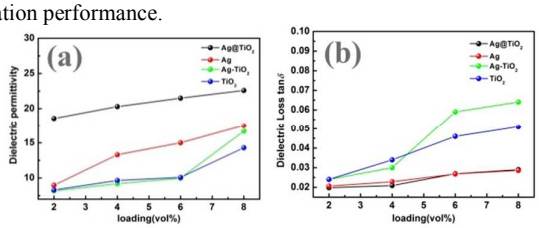

Fig. 6 Comparison of dielectric properties for P (VDF-HFP) hybrid films with Ag@TiO_2, Ag, Ag-TiO_2 and TiO_2 at 1 KHz: (a) Dielectric permittivity and (b) dielectric loss

Figure 6 illustrates the dielectric properties of P (VDF-HFP)/Ag@TiO_2, P (VDF-HFP)/Ag, P(VDF-HFP)/TiO_2 and P (VDF-HFP)/Ag/TiO_2 hybrid films at 1 KHz. Considering that the P (VDF-HFP)/Ag composite can be easily changed from insulator to conductor, the comparison is performed at a low concentration range from 2vol%-8vol%. It was found that both dielectric constant and tan δ increase gradually with filler content increase. As shown in Figure 6(a), it is worth noting that the Ag@TiO_2 composites exhibit higher dielectric constant compared with pure Ag composites , pure TiO_2 composites and Ag/TiO_2 blend composites presumably on account of introduction by TiO_2 insulating layer. As Ag was coated by TiO_2 layer, the interfacial area inside the nanocomposites has been enlarged because of the hybrid nanofillers, which is considered to enhance the duplex interfacial polarizations and endows composites with higher dielectric constant than others which only embedded pure nanoparticles [42]. Additionally, composite with conductive fillers perform higher dielectric permittivity than ceramics one at relatively low loading for the micro-capacitance effect [4]. It can be observed from Figure 6(b) that Ag@TiO_2 composite has a little smaller or nearly the same dielectric loss as the composite including pure Ag (below 0.03 at 1K Hz). Composites include TiO_2 nanoparticles show obviously bigger dielectric loss, which is similar to the previous research [43-44]. In our work, the Ag nanoparticles can be isolated by the ultrathin TiO_2 layer so that direct contact among conductive Ag particles can be suppressed to some extent, which reduce the conductivity and keep the dielectric loss pretty low. It also verified that an obvious increment of dielectric permittivity can be achieved maintaining a low loss by

filling Ag@TiO_2 core-shell structure nanoparticles into P (VDF-HFP) matrix.

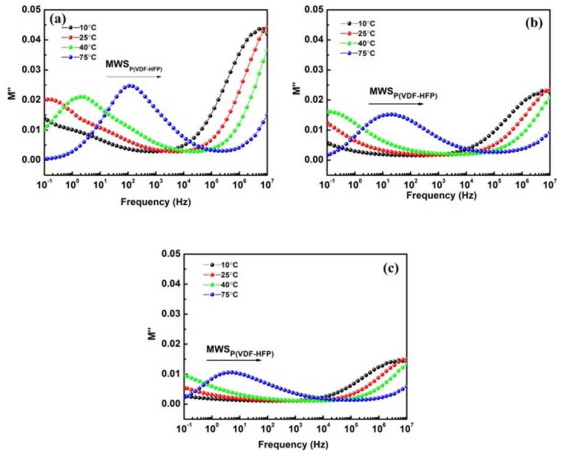

Fig.7. Frequency dependence of electrical modulus (M'') of (a) pure P(VDF-HFP), (b) Ag/P(VDF-HFP) (6vol%) and (c) Ag@TiO_2/P(VDF-HFP) (6vol%) composites measured at different temperatures.

Electric modulus is used to study dielectric relaxation processes of the composites and evaluate the influence of fillers on the relaxation behavior of polymer matrix. As is shown in Figure.7, all of the samples consisted by pure P(VDF-HFP), P(VDF-HFP) /Ag, P(VDF-HFP)/TiO_2 and P(VDF-HFP)/Ag@TiO_2 composites display the same interfacial polarization or $MWS_{P(VDF-HFP)}$ effect, which is a relaxation process appearing in heterogenous systems due to accumulation of charges at the interface of the system. As the matrix/nanoparticle interface charges form large dipoles, it is unable to follow simultaneously the alternation of the applied electric field [45]. The peaks are also shift to high frequency as the temperatures increases, namely a typical characteristic of MWS polarization [46]. In the electric modulus presentation, the intensity of loss peaks is expected to decrease with increasing filler content. This can be identified by simply comparing the results from the pure P (VDF-HFP) and sample with Ag@TiO_2/P (VDF-HFP) (6vol %). Compared with pure P (VDF-HFP) and Ag/P (VDF-HFP), Ag@TiO_2/P (VDF-HFP) composite shows the lowest relaxation intensity, indicating the TiO_2 shell layer can further suppresses the space charge accumulation in the polymer matrix.

Conclusions

In summary, Ag@TiO_2 core–shell nanoparticles can be fabricated by a vapor-thermal method as functional fillers. The hybrid films with homogeneously dispersed Ag@TiO_2 nanoparticles in the ferroelectric P (VDF-HFP) matrix were first prepared. Thermal analysis indicate that introduction of Ag@TiO_2 does not disrupt the process of polymer matrix while the well dispersed Ag@TiO_2 nanoparticles lead to more nucleation sites and facilitates the nucleation. Moreover, as-synthesized Ag@TiO_2/ P (VDF-HFP) composites are equipped with higher thermal stability than pure P (VDF-HFP). The P (VDF-HFP)/Ag@TiO_2 composite exhibited enhanced dielectric properties and the dielectric permittivity of polymer nanocomposites is enhanced by~300% over the P(VDF-HFP) matrix at a low filler loading of 10vol%. Moreover, the P(VDF-HFP)/Ag@TiO_2 also exhibited higher dielectric constant than P(VDF-HFP)/Ag, P(VDF-HFP)/TiO_2 and P(VDF-HFP)/Ag/TiO_2 blend composite while maintaining a low loss tangent(below 0.03 at 1KHz) for duplex polarizations effect. These enhanced properties may allow more capability of PVDF-based polymer matrix composites as smart functional materials for embedded devices in the electronic industry.

Acknowledgements

The authors gratefully acknowledge the financial support from the National High Technology Research and Development Program of China (863 Program) (No. 2013AA030701) and the Fundamental Research Funds for the Central Universities (No. 2015QNA4007).

Notes and references

School of Materials Science and Engineering, State Key Lab Silicon Mat, Zhejiang University, Hangzhou 310027, PR China
* Corresponding author. Email: mse237@zju.edu.cn

1 Y. S, Y. H. Lin, M. Li and C. W. Nan, *Adv. Mater.*, 2007, **19**, 1418-1422
2 S. H. Liu, S. X. Xue, W. Q. Zhang, J. W. Zhai, G. H. Chen, *J. Mater. Chem A.*, 2014, **2**, 18040-18046.
3 Y. Shen, Y. H. Lin and C. W. Nan. *Adv. Funct. Mater.* , 2007, **17**, 2405-2410
4 Z. M. Dang, J.K. Yuan, J.W. Zha, T. Zhou, S. T. Li and G. H. Hu, *Progress in Materials Science.*, 2012, **57**, 660-723
5 A. Datta, D. Mukherjee, S. Witanachchi and P. Mukheerjee. *Adv. Funct. Mater*., 2014, **24**, 2638-2647.
6 H. X. Tang and H. A. Sodano. *Nano. Lett*., 2013, **13**, 1373-1379.
7 L. Y. Xie, X. Y. Huang, S. T. Li and P. K. Jiang. *J. Mater. Chem A.*, 2014, **2**, 5244-5251
8 B.H. Fan, J.W. Zha, D. R. Wang, J. Zhao and Z. M. Dang. *Appl. Phys. Lett.*, 2012,**100**, 012903
9 E.Q. Huang, J. Zhao, J. W. Zha, L. Zhang, R.J. Liao and Z. M. Dang. *J. Appl. Phys*., 2014,**115**, 194102
10 Y. Yang, B. P. Zhu, Z. H. Lu, Z. Y. Wang, C.L. Fei, D. Yin, R. Xiong, J. Shi, Q. G. Chi and Q. Q. Lei. *Appl. Phys. Lett*., 2013**, 102**, 042904
11 X. Zhang, W. W. Chen, J. J. Wang, Y. Shen, L. Gu, Y. H. Lin and C. W. Nan, *Nanoscale.*, 2014, **6**, 6701-6709.
12 D. Yu, N. X. Xu, L. Hu, Q. L. Zhang and H. Yang. *J. Mater. Chem. C.* 2015, **3**, 4016- 4022.
13 Q. G. Chi, J. Sun, C. H. Zhang, G. Liu, J. Q. Lin, Y. N. Wang, X. Wang and Q. Q. Lei, *J. Mater. Chem C* ., 2014, **2**, 172-177.
14 L. Qi, B.I. Lee, S. Chen, W.D. Samuels and G.J. Exarhos. *.Adv. Mater.* , 2005, **17**, 1777–1782.
15 A. B. da Silva, M. Arjmand, U. Sundararaj and R. E. S. Bretas. *Polymer.* , 2014, **55**, 226-234
16 D. R. Wang, Y.R. Bao, J. W. Zha, J. Zhao, Z. M. Dang and G. H. Hu. *ACS Appl. Mater. Interfaces.*,2012, **4**, 6273−6279
17 Z. M. Dang, L. Wang, Y. Yin, Q. Zhang and Q.Q. Lei. *Adv. Mater.*, 2007, **19**, 852–857
18 Y. Yang, H. L. Sun, D. Yin, Z. H. Lu, J. H. Wei, R. Xiong, J. Shi, Z. Y. Wang , Z. Y. Liu and Q. Q. Lei. *J. Mater. Chem. A.*, 2015, **3**, 4916–4921
19 T. Wei, C. Q. Jin, W. Zhong and J.M. Liu. *Appl. Phys. Lett.*, 2007**, 91**, 222907

20 L. Zhang, S. Y. Yuan, S. Chen, D. R.Wang, B. Z. Han and Z. M. Dang, *Comp. Sci. Tech*., 2015, **110**, 126-131.
21 W. Zheng, X. F. Lu, W. Wang, Z. J. Wang, M. X. Song, Y. Wang and C. Wang, *Phy. Staus Solidi A*., 2010, **207**, 1870-1873
22 X. W. Kuang, Z. Liu and H. Zhu, *J. Appl. Polym. Sci.*, 2013,**129**, 3411–3416.
23 X. W. Liang, S. H. Yu, R. Sun, S. B. Luo and J. Wan, *J. Mater. Res*., 2012, **27**, 991-998
24 Q. H. Zhang, W.G. Fan and L. Gao. *Appl. Catal. B.*, 2007, **76**, 168–173.
25 Y. R. Su, J. G. Yu and J. Lin. *J. Solid. State. Chem.*, 2007,**180**, 2080–2087.
26 X. X. Yu, J. G. Yu, B. Cheng and M. Jaroniec. *J. Phys. Chem. C,* 2009, **113**, 17527–17535
27 J. G. Yu, G. H. Wang, B Cheng and M. H. Zhou, *Applied Catalysis B: Environmental,* 2007, **69**, 171–180
28 J. G. Yu, J. F. Xiong, B. Cheng and S. W. Liu, *Applied Catalysis B: Environmental,* 2005, **60**, 211–221
29 G. M. Liu, W. Jaegermann, J. J. He, V. Sundstrom and L. C. Sun**.** *J. Phys. Chem. B,* 2002, **106***,* 5814-5819
30 H. Zhang, G. Wang, D Chen, X. J. Lv and Jinghong Li. *Chem. Mater*. 2008, **20**, 6543–6549
31 U. Diebold and T. E. Madey. *Surface Science Spectra*, 1996, **4**, 227-231
32 J. M. Du, J. L. Zhang, Z. M. Liu, B. X. Han, T. Jiang and Y. Huang. *Langmuir*, 2006**, 22***,* 1307-1312
33 T. Kasuga, H. Kondo and M. Nogami. *Journal of Crystal Growth*., 2002, **235**,235–240
34 R. Sanjinés, H. Tang, H. Berger, F. Gozzo, G. Margaritondo and F. Lévy. *J.Appl. Phys*., 1994,**75**, 2945-2951
35 X. Y. Huang. Study on the properties and preparation of polyethylene aluminum nanocomposite dielectrics [D]. Shanghai Jiao Tong University, 2008
36 S. H. Liu, J. W. Zhai, J. W. Wang, S. X. Xue and W. Q. Zhang. *ACS Appl. Mater. Interfaces*., 2014, **6**, 1533-1540.
37 K Yang, X. Y. Huang, L.J. Fang, J. L. He and P. K. Jiang, *Nanoscale*, 2014, **6**, 14740–14753
38 E. E. Shafee, M. E. Gamal and M. Isa. *J. Polym. Res.,* 2012, **19**, 9805-8
39 Q. Wang and L. Zhu. *J. Polym. Sci. Part B: Polym .Phys.,* 2011, **49**, 1421–9.
40 W. Zheng, X. F. Lu, W. Wang, Z. J. Wang, M. X. Song, Y. Wang and C Wang, *Phys. Status Solidi A*., 2010, **207**,1870–1873
41 F. X. Guan, J. L. Pan, J. Wang, Q. Wang and L. Zhu, *Macromolecules*., 2010, **43**, 384–92
42 Y. Zhang, Y. Wang, Y. Deng, M. Li and J. B. Bai, *ACS Appl. Mater. Interfaces.*, 2012,4,65-68
43 J. J. Li, S. I. Seok, B. J. Chu, F. Dogan, Q. M. Zhang and Q. Wang, *Adv. Mater*. 2009, **21**, 217–221
44 H. X. Tang and H. A. Sodano. *Appl. Phys. Lett.,* 2013,**102**, 063901
45 G. A. Kontos, A. L. Soulintzis, P. K. Karahaliou, G. C. Psarras, S. N. Georga, C. A. Krontiras and M. N. Pisanias. *eXPRESS Polymer. Letters*., 2007, **1**, 781–789
46 L. Y. Xie, X. Y. Huang, B. W. Li, C. Y. Zhi, T. Tanaka and P. K. Jiang. *Phys. Chem. Chem. Phys.*, 2013, **15**, 17560-17569.